Review Paper

Chemical surface and thin film analysis in glass coating[1)]

Hans Oechsner

Institut für Oberflächen- und Schichtanalytik (IFOS), Universität Kaiserslautern (Germany)

After a short overview of recent analytical techniques for compositional surface analysis and the determination of concentration depth profiles, the principle, the instrumentation and the performance of the routinely used electron spectroscopic and mass spectrometric methods, namely photo- and Auger electron spectroscopy as well as secondary ion and secondary neutral mass spectrometry, are described. The application of these techniques to electrically insulating surfaces and layer structures is particularly emphasized by corresponding practical examples. Secondary neutral mass spectrometry is specifically addressed with regard to the potentialities of the novel high-frequency mode of electron-gas secondary neutral mass spectrometry for quantitative composition analysis and high-resolution depth profiling of electrically nonconducting sample structures.

Chemische Oberflächen- und Dünnfilmanalyse bei der Glasbeschichtung

Nach einem Überblick über die Methoden zur Bestimmung der chemischen Zusammensetzung von Oberflächen und zur Ermittlung von Konzentrationstiefeprofilen werden das Prinzip, die instrumentelle Realisierung und die Arbeitsweise der routinemäßig eingesetzten elektronen- und massenspektrometrischen Methoden, nämlich der Foto- und der Auger-Elektronenspektroskopie sowie der Sekundärionen- und Sekundärneutralteilchen-Massenspektrometrie, beschrieben. Dabei werden insbesondere die Möglichkeiten zur Anwendung dieser Methoden auf dielektrische Proben und Schichtstrukturen anhand von praktischen Beispielen behandelt. Im speziellen werden die Möglichkeiten dargestellt, die sich mit der neuentwickelten Hochfrequenzmethode der Sekundärneutralteilchen-Massenspektrometrie auf der Basis der Nachionisation in einem heißen Elektronengas ergeben.

1. General overview

With decreasing dimensions and increasing sophistication of the architecture of glass coatings the traditional techniques for the chemical characterization of materials have to be mandatorily replaced with such techniques which combine quantitative chemical analysis with high depth resolution. Also the precise characterization of the glass surface on which a layer structure is built up is a necessary prerequisite for guaranteeing the desired qualities of a coating, as for instance its adhesion. In particular, the knowledge of the conditions and the behavior of the interfaces at the glass substrate and within a layered structure are decisive for the functional properties of a coating.

The relevant information can be supplied by analytical techniques which have evolved from the field of surface physics. Such methods are based on the excitation of surface-sensitive analytical signals through the interaction of photons, electrons or ions with the outermost atomic layers of a sample. There is distinguished, in particular, between two main groups, i.e.

- electron spectroscopic techniques such as Photoelectron (PES) or Auger electron spectroscopy (AES) by which the analytical information is derived from the kinetic energy of electrons released from surface atoms or surface-near electronic bands, and
- mass spectrometric methods such as secondary ion (SIMS) or secondary neutral mass spectrometry (SNMS) characterizing charged or neutral atoms and molecules released from the sample surface.

Besides these methods numerous other techniques for the chemical, but also for the structural characterization of solid surfaces have been developed, e.g. [1 to 6]. Thus, the spectral characterization of the light emitted during the ion bombardment of a glass surface can deliver useful information about the surface-near composition [7]. Backscattering methods enable the mass of surface particles to be derived from the loss of kinetic energy which impinging and subsequently backscattered particles experience during their interaction with the surface [8]. Detailed chemical information about the short-range atomic order or even the atomic neighborhood conditions in a solid are possible as well, e.g. by a careful inspection of the fine structure near X-ray adsorption edges (Extended X-ray Adsorption Fine Structure (EXAFS) [9]). Recent scanning probe techniques such as Scanning Tunneling Microscopy (STM) or Atomic Force Microscopy (AFM) do not only supply infor-

Received March 13, revised manuscript August 19, 1997.

[1)] Presented as "Short course" at: 1st International Conference on Coatings on Glass, October 27 to 31, 1996 in Saarbrücken (Germany).

mation about the nanostructural or even the atomic order also on nonconducting surfaces, but deliver to some extent also local chemical information when being operated in a spectroscopic mode [10]. The author will, however, concentrate here on such techniques for chemical surface analysis which have become of practical importance to a larger extent.

The analysis of thin films becomes possible when such methods are combined with an appropriate microsectioning technique [11]. Besides mechanical bevelling methods as a well defined grinding with a rotating sphere, the controlled sputter removal of the surface by low-energy ion bombardment has become the most widely applied method in that context. Under careful operation, sputter erosion enables compositional depth profile analysis almost along an atomic scale.

When ion sputtering is employed either for depth profiling or to remove contamination layers from the surface to be analyzed, an important difference between the above-mentioned groups of analytical techniques has to be taken into account: While the electron spectroscopic techniques are detecting what is left at the surface after it has been attacked by the ion bombardment, the signals obtained with the mass spectrometric techniques refer to those particles which are leaving the surface. This makes both groups of methods complemental to each other.

The analytical information obtained with either of these techniques may differ considerably, since a preferential removal of certain species from the surface through the ion bombardment can sometimes cause drastic deviations from the original surface composition. In that respect, a mass spectrometric method like SNMS collecting the removed surface particles with specific, but well-defined detection probabilities may be more beneficial.

As another general aspect, the large differences between the detection power of the individual techniques have to be considered: Electron spectroscopic methods such as AES or PES are in general confined to a detection power of at best several tenths of an atomic percent, i.e. concentrations of 10^{-2} to 10^{-3}. On the contrary, mass spectrometric surface analytical techniques provide always detection powers in the ppm range; sophisticated SIMS or SNMS instruments enable one even to detect concentrations down to the ppb regime.

Since in all analytical techniques being dealt with here an electrical charge is either brought to or removed from the sample surface via the probing or the detected species, they can readily be applied to sample structures of sufficient electrical conductivity. Special additional measures, however, have to be implemented for the analysis of a non- or poorly conducting substrate like glass, or even more mandatorily, when the coating consists entirely or in part of dielectric material. In order to make surface-analytical techniques, especially in conjunction with sputter depth profiling, applicable to such sample structures, emphasis must be paid on how to compensate any surface charging which would deteriorate either the characteristic electron energies in AES or PES or prevent any controlled sputter removal by decelerating the bombarding ions.

In the following sections the surface-sensitive character of the electron and mass spectrometric techniques will be discussed as well as the possibilities for high-resolution sputter depth profiling. The physical background and the experimental procedure of the different techniques will be described, particularly with regard to their application to nonconducting samples. Recent methodical progress which is not yet included in available textbooks or reviews on surface and thin film analysis will be addressed where appropriate with regard to the analysis of dielectric, i.e. electrically insulating structures.

2. Conditions for surface-sensitive chemical analysis and high-resolution depth profiling

2.1 Surface sensitivity

Electrons released from element-specific atomic energy levels or atomic bands can only deliver the desired information about the respective species when they leave the sample surface with their original energy. Hence, they must not experience any inelastic processes in the solid until crossing the vacuum energy level. This requirement establishes the high surface sensitivity of the electron spectroscopic methods PES and AES. The "elastic" escape depth or "inelastic free path" of photo- or Auger electrons is for statistical reasons exponentially decaying with the depth z from the surface of a "random" sample, i.e. when the influence of single crystalline effects can be neglected. The electron escape function can then be described by $f_{esc} = \exp(-z/\lambda(E))$, where $\lambda(E)$ is the mean electron escape depth or the inelastic mean free path for electrons originating with an energy E through photoionization or Auger processes. The variation of λ with the electron energy E follows with a relatively small scatter a uniform curve being depicted in figure 1. For electron energies in the order of a few 100 eV, λ is only in the order of a few atomic distances. Photoelectron and Auger electron spectroscopy measuring the original electron energies are thus probing only the atoms in the outermost atomic layers, and hence, the surface composition.

The universal curve for the electron inelastic mean free path can be in a good approximation described by the relation [12]

$$\lambda(E) = A\,E^{-2} + B(a\,E)^{0.5}\,. \qquad (1)$$

$\lambda(E)$ is obtained in terms of monolayers when the electron energy E is given in eV. The quantity a describes the monolayer thickness in nm. The coefficients A and B amount to 538 and 0.41 for elements, or to 2170 and 0.72 for inorganic compounds [1, p. 209].

The information depth of the mass spectrometric techniques SNMS and SIMS is comparable with $\lambda(E)$ or even more shallow. This has been demonstrated by computer simulations of the interaction of energetic particles with solid surfaces [13], or experimentally by the depth resolution with which atomically sharp interfaces, for example in carefully prepared multilayer structures of short-range ordered material, can be probed. An example is given in figure 2. By SNMS depth profiling with normally incident Ar^+ ions of only 200 eV the experimental 84 to 16% interface width between two sublayers in a silicon–tantalum multilayer structure has been found to be in the order of only 1.5 nm [14]. This agrees well with the physical limit given by the atomic roughness arising from the statistics of the removal of surface atoms during the sputter process. From corresponding simulations such atomic roughnesses are found to be in the order of 4 to 5 atomic distances which agrees well with the best interface widths obtained in sputter depth profiling. Hence, an experimental transition width as in figure 2 cannot only be assumed to describe an atomically sharp interface, but demonstrates simultaneously that for sufficiently low primary ion energies the particles being analyzed with SNMS or SIMS are almost completely released just from the outermost atomic layer.

2.2 Experimental techniques for high-resolution depth profiling

For relatively thick layer structures bevelling or tapered-section techniques can be applied successfully to obtain depth-dependent chemical information across the layer thickness. Tapering can be achieved by appropriate machining such as, for instance, the formation of a flat bowl with a rotating ball. Extremely flat bevelling angles down to $10^{-4°}$ to $10^{-5°}$ can also be realized by sputter erosion with an ion beam of slight divergence, i.e. a minute lateral variation of the ion current density.

The depth resolution achieved across a tapered section can be estimated from figure 3. When an ideally sharp interface between two sublayers I and II, or between a coating and a substrate is probed by an analyzing electron or ion beam of diameter d_b, the (absolute) depth resolution Δz is given by [11]

$$\Delta z = d_b \sin\alpha + \delta l \cos\alpha \,, \tag{2}$$

where α is the bevelling angle and δl is the information depth of the analytical technique (see section 2.1). Δz becomes smallest when the influence of the larger of the two quantities d_b or δl is minimized via the choice of the bevelling angle α. Since in most cases the information depth δl is below the beam diameter d_b, a depth resolution Δz close to the information depth is obtained for $\alpha \to 0$. Therefore, bevelling angles well below 1° should be used when cutting mechanically through a thick layer structure.

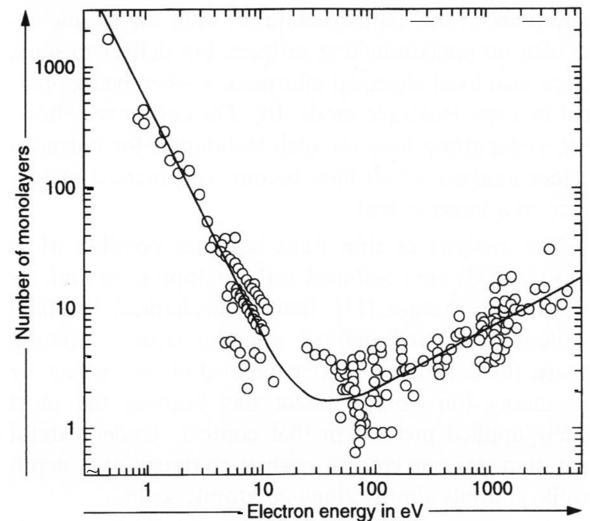

Figure 1. Experimental data of elastic mean electron escape depth or inelastic mean free electron paths in solids [12].

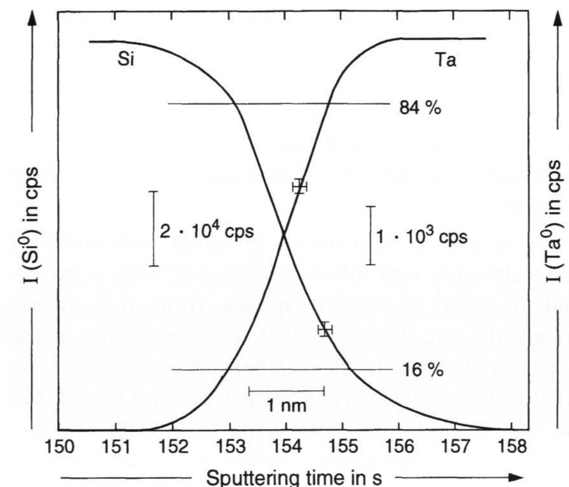

Figure 2. Sputter depth profile measured with secondary neutral mass spectrometry across a sublayer interface in a silicon–tantalum multilayer structure [14].

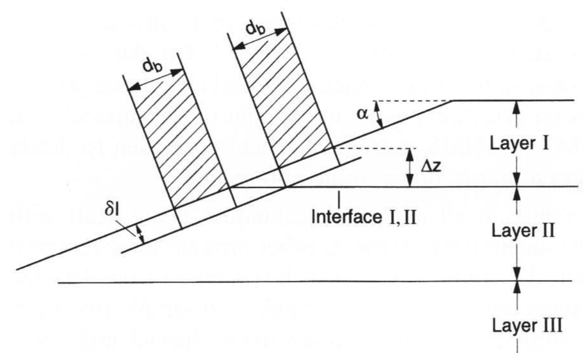

Figure 3. Principle of depth profile analysis by the tapered-section or bevelling method.

It can be readily seen from equation (2) that for small δl values a sample removal parallel to the film plane, i.e. with $\alpha = 0$, is most favorable. In that case ion sputtering

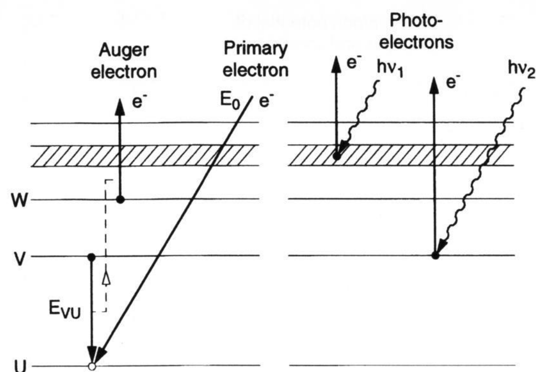

Figure 4. Schematic of the fundamental processes for photo- and Auger electron spectroscopy.

is the most appropriate microsectioning technique. However, special precautions are mandatory to eliminate deteriorating influences from so-called crater effects, i.e. from a curved bottom of the sputtering crater, or from signal contributions from the crater walls. Lateral inhomogeneities of the bombarding ion current density have, therefore, to be strictly avoided. This can be achieved by rastering an ion beam across the analyzed area or, even more advantageously, by low-energy ion bombardment from a low-pressure plasma when an extremely plane extraction geometry is established [15]. The latter method is used in the so-called direct bombardment mode of SNMS (see section 4.2). The example shown in figure 2 has been obtained with this technique.

Signal contributions from the crater walls can be suppressed for AES when the narrow probing electron beam is directed preferentially to the center of the ion beam raster area, or for SIMS and SNMS when by an appropriate gating technique signal recording is only performed when the raster-scanned ion beam hits the center of the sputter crater. In the direct bombardment mode of SNMS contributions from the crater walls can be well suppressed when the diameter of the bombarded area becomes large enough, so that again only its central part is "seen" by the entrance aperture of the detection system.

Depth resolution in sputter profiling can further be deteriorated by a number of effects as the development of a bombardment-induced surface microtopography due to structural or chemical inhomogeneities of the sample [16], by collisional atomic mixing effects which may smear out sharp interfaces in the analyzed film structure, and a delayed or preferred sputter removal of different sample constituents. The latter effect does not only result in a delayed signal decay when profiling across an interface, but is even more important in view of the resulting variations of the surface composition due to preferential sputtering effects. As already mentioned in section 1., this may lead to strong differences in the analytical information obtained with electron spectroscopic techniques on the one hand and mass spectrometric methods on the other.

Optimum depth resolution is quite obviously obtained when atomic mixing effects are avoided, i.e. when energy deposition through the ion bombardment is confined to the information depth of the respective analytical method. Hence, a low energy and/or a high mass of the bombarding ions resulting in a very limited range of the impinging ions in the solid is most preferable. Because of large angle scattering effects between primary particles and sample atoms, such conditions can be established rather incompletely by an oblique incidence of a high-energy ion beam. Sample rotation under oblique ion bombardment has been proposed as another method to improve depth resolution [17]. This technique leads indeed to sharply detected interfaces. One has, however, to be aware that because of a kind of sputter polishing rough interfaces may then appear much sharper than existing in the real sample structure.

3. Electron spectroscopic methods for surface analysis

3.1 Photoelectron spectroscopy

3.1.1 Physical background and instrumentation

The basic mechanisms of electron emission stimulated by photon or electron irradiation are schematically shown in figure 4. The PES signals result from the photoionization process in a certain energy level in the atomic core, a valence band or the conduction band. An ionization in a core level can also be followed by a rearrangement of the electronic structure which may lead to the emission of an Auger electron in a radiationless process. Therefore, in electron energy spectra resulting from the irradiation with photons of sufficient energy (soft X-rays) Auger electron peaks do always appear besides the photoelectron peaks. Since Auger electron emission is independent of the kind of the primary ionization event, photoelectron peaks can be readily discriminated against the Auger peaks by a variation of the energy of the irradiating photons.

Depending on the energy of the incident photons and, hence, the regime of the electron binding energy which is probed, it is distinguished between Ultraviolet Photoelectron Spectroscopy (UPS) and X-ray-induced Photoelectron Spectroscopy (XPS). While UPS, employing photon energies of 10 to 40 eV, has become an important tool for the determination of electronic band structures and the characterization of adsorbate systems, XPS using in general the excitation with the $MgK_{\alpha 1,2}$ line (1253.6 eV) or the $AlK_{\alpha 1,2}$ line (1486.6 eV) probes element-specific electronic core levels (and was hence originally denoted as Electron Spectroscopy for Chemical Analysis (ESCA)). As an important condition for the identification of specific electron binding energies, E_b, the line width is sufficiently small in both cases (0.7 and 0.85 eV, respectively).

Besides the photon source – a gas discharge lamp mostly operated with helium or neon in the case of UPS or a low-energy X-ray tube for XPS – an electrostatic

energy analyzer with an electron-counting system is the other essential component of a PES apparatus. Most frequently a hemispherical analyzer is used. According to figure 5 the electron energy at the entrance of the analyzer system is given by

$$E_k = h\nu = E_b^F = \Phi_{sp} , \quad (3)$$

where E_b^F is the respective electron-binding energy related to the Fermi level of the sample material, and Φ_{sp} the (fictive) spectrometer work function being a constant of the PES apparatus. For a fixed photon energy $h\nu$ and after the determination of Φ_{sp} via a standard sample (mostly gold with E_b^F = 83.98 eV for the $4f_{7/2}$ electron energy level) the element-specific electron-binding energies E_b^F can be determined from the measured E_k values, both varying inversely to each other.

The hemispherical energy analyzer of a PES apparatus is in general preceded by an electron optical deceleration system by which the electrons are preretarded before entering the analyzer. The complete system can be operated in two modes:

a) In the so-called fixed retardation ratio mode (FRR) the electrons are retarded to the central ray energy E_0 of the analyzer such that E_k/E_0 = const. In this mode the energy resolution $\Delta E/E$ is constant and the absolute resolution ΔE is improved by shifting E_k to a lower, variable path energy E_0. The analyzer transmission T is proportional to E_0 and, hence, to E_k in this case.

b) In the fixed analyzer transmission mode (FAT mode) the electrons are decelerated always to a fixed central ray energy E_0 which results quite obviously in a constant absolute energy resolution ΔE. The analyzer transmission T in that case is proportional to E_0^2/E_k.

The electron intensity arriving at the counting element (multiplier or channel plate) is given by $I_c \sim T \cdot N(E)$, where $N(E)$ is the height of the electron energy distribution around an energy E. Then, the XPS signals are proportional to $N(E_k) \cdot E_k$ in the FRR mode, but to $N(E_k)/E_k$ in the FAT mode, when the electron deceleration is assumed not to change the original energy distribution.

3.1.2 Quantification of PES

Figure 6 displays the XPS spectrum for a contaminated glass surface. The respective measurement was performed in the FAT mode with a fixed analyzer path energy of 117.4 eV. The E_k axis has already been transferred into that for the electron-binding energy E_b^F according to equation (3). Apart from the photoelectron peaks (for instance the O 1s or the Na 1s peaks) the spectrum contains Auger electron peaks (O KVV or C KLL) as expected.

The photoelectron signal from a sample that is homogeneous in the analysis volume can be written in a simplified form as

$$I_X^{PES} = j_{h\nu} \cdot n_X \cdot \sigma_X \cdot \lambda_X \cdot T \cdot F , \quad (4)$$

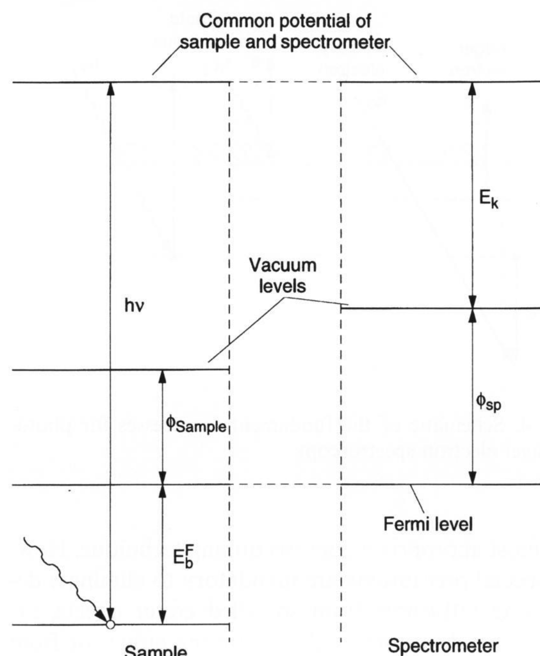

Figure 5. Relation between the measured kinetic electron energy E_k and the electron binding energy E_b^F in photoelectron spectroscopy. (A corresponding scheme applies to Auger electron spectroscopy.)

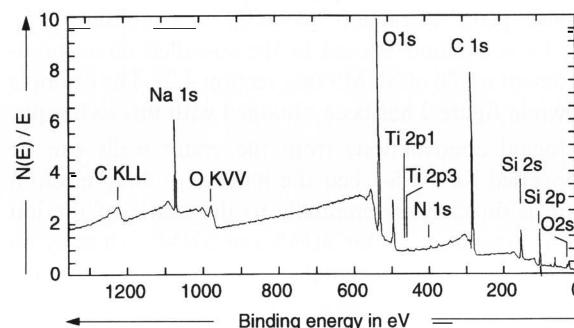

Figure 6. XPS spectrum for a contaminated glass surface (excitation by AlK_α, analyzer pass energy 117.4 eV in the FAT mode). (Measurement by K. Berresheim, IFOS.)

where $j_{h\nu}$ is the incident photon flux density (in general 10^{12} photons/(cm^2 s)), n_X the number of atoms of element X per cm^3, σ_X the photoionization cross-section for the considered orbital of X, λ_X the mean escape depth (inelastic mean free path) of the respective photoelectrons, T the analyzer transmission, and F a geometry and efficiency factor of the individual PES instrument. When the factors being characteristic of the excitation of a certain photoelectron peak and the individual apparatus are combined to a detection factor S_X, equation (4) can be rewritten as

$$n_X = I_X^{PES}/S_X . \quad (5)$$

Finally, from the individual n_i values for all different elements in the analysis volume the concentration of X is obtained as

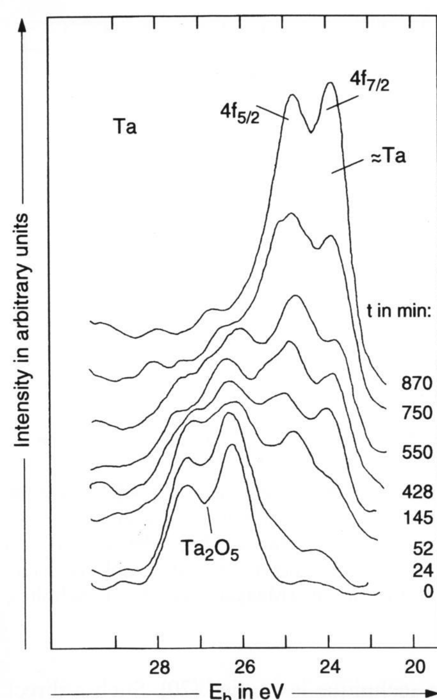

Figure 7. Chemical shift of the $4f_{5/2}$ (left) and $4f_{7/2}$ (right) photoelectron peaks from XPS analysis during the sputter removal of a Ta_2O_5 film on tantalum with 2 keV Ar^+ ions. (t = 0 refers to Ta_2O_5, t = 870 min to pure tantalum.) (Measurement by J. Sopka, Universität Kaiserslautern.)

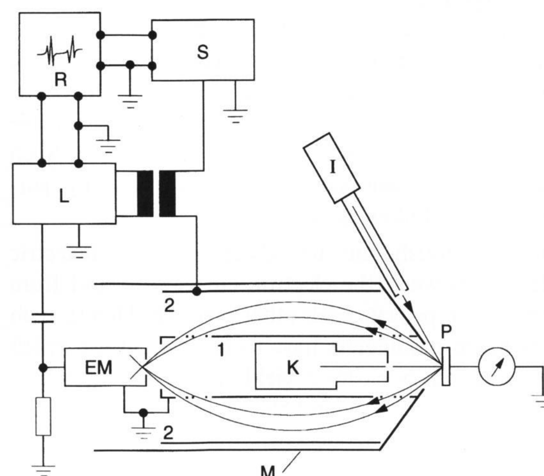

Figure 8. Scheme of an AES apparatus with a cylindrical mirror analyzer. EM: electron multiplier, I: ion gun, K: coaxial electron gun, L: lock-in amplifier, M: magnetic shield, P: sample, R: spectrum recorder, S: saw-tooth generator for scanning across the Auger electron spectrum; 1,2: cylindrical mirror electrodes.

$$c_X = \frac{n_X}{\sum n_i} = \frac{I_X/S_X}{\sum I_i/S_i} . \qquad (6)$$

For the quantification according to equation (6) I_X (or I_i) has to be taken as the total count rate of the considered photoelectron peak, i.e. the area of the peak after subtracting the background signal in an appropriate way, most simply by a linear interpolation between the two footpoints of the peak. A corresponding evaluation of the XPS spectrum in figure 6 yields, e.g., an oxygen concentration (in at. %) of 30.4 and a carbon concentration of 49.7 at the contaminated surface.

An important aspect of the XPS method is the possibility of getting information about the chemical state of an atomic species by a chemical shift of the individual photoelectron peaks. This effect results from the change of the energetic structure of the electron system resulting from the charge transfer during the formation of a chemical bond. It is this possibility which makes XPS, in particular, useful not only for the compositional characterization, but also for the detection of the binding conditions at a sample surface. In a dynamic mode, surface reactions as, e.g. the oxidation process can be monitored. An example is given in figure 7 for a variation of the Ta 4f peaks when a thin Ta_2O_5 layer on a polycrystalline tantalum surface is sputter-removed under bombardment with Ar^+ ions of 2 keV. Depending on the energy resolution of the electron spectrometer even the individual binding states of carbon in different hydrocarbons can be detected, e.g. [1].

The application of PES to nonconducting samples does in general not cause serious problems when the photoelectron flux from the sample remains relatively small. Even for a slight charging up XPS spectra remain evaluable, as the whole spectral structure is just shifted uniformly along the energy axis. In such cases, the chemical characterization of an insulating surface or coating can still be performed in a reliable manner when the energetic differences of the individual photoelectron peaks are used for their identification making use of corresponding tables or handbooks such as [18].

3.2 Auger electron spectroscopy

3.2.1 Instrumentation and experimental procedure

According to figure 4 three different atomic energy levels are involved in the formation of an Auger electron. Hence, AES can identify elements with an atomic number $Z \geq 3$ (i.e. starting with lithium). Recent AES instruments are mostly based on a so-called Cylindrical Mirror Analyzer (CMA) (figure 8). Since a CMA accepts the ejected electrons in a 2π geometry in a cone mantle with a half-opening angle of 42.3°, it yields relatively high signal intensities. Other types of electrostatic analyzers are also employed, particularly when AES is combined with in-situ PES. Retarding field analyzers can be employed as well, in order to combine chemical analysis with structural surface information from Low Energy Electron Diffraction, LEED, e.g. [3].

In CMA-based instruments the primary electron gun is in general located inside the inner cylinder of the analyzer, and the exciting electron beam is travelling along the cylinder axis. Then, the sample can be readily positioned in such a distance to the analyzer entrance for which optimum conditions for the electron trajecto-

ries through the analyzer are achieved. Auger signals are recorded both in a direct mode displaying the electron energy distributions $N(E)$ for the individual peaks, or as differentiated spectra which increase in general the detection sensitivity and enable a simple separation of the background from the "true" secondary electrons. CMA systems are mostly operated without any preretardation system, i.e. with $\Delta E/E$ = const. Therefore, the Auger intensities measured in the direct mode are proportional to $E \cdot N(E)$ (see also section 3.1). In contrast to the "analogue" version of an AES instrument as displayed in figure 8, direct data storage and handling by a computer system becomes increasingly employed in recent AES equipment.

3.2.2 Quantification of AES

The quantification of AES follows the same routes as for PES (section 3.1.2). Quite evidently, the formation probability for an Auger electron has now to replace the photoionization cross-section in equation (4). Also, the deceleration of the primary electrons within the sample depth from which Auger electrons are escaping, and the contribution of elastically backscattered primary electrons contributing to the formation of Auger electrons have to be considered.

As in the case of X-ray-induced photoelectron spectroscopy the individual electron peaks are identified by a comparison with tabulated values from standard handbook spectra, e.g. [19]. For the determination of the concentration of an element X from a particular characteristic Auger peak, equation (6) can be applied again. Mostly, the sensitivity factors S_i which refer now to a certain Auger transition are conveniently replaced by relative sensitivity factors referring all S values to that for one reference Auger peak. Thus, the individual experimental parameters or their variation during the analysis must not be taken into account separately. As for PES, the areas of the Auger electron peaks have to be determined when the Auger electron spectra are recorded in the direct mode. For the differentiated Auger spectra the peak-to-peak (ptp) amplitudes can be taken as the Auger intensities I_X entering equation (6), since for a Gaussian or Lorentzian shape of the Auger peak the ptp amplitude is directly proportional to the area of the undifferentiated peak.

Besides the use of absolute or relative sensitivity factors as tabulated in handbooks, their determination from standards is sometimes a better solution for an individual sample. In an elegant way the relevant sensitivity factors can be determined from so-called correlation plots for a sample of varying stoichiometry, i.e., when following, for instance, the AES intensities across an interface during sputter profiling. When the AES signals for two elements are plotted against each other, the respective S values are delivered by the intersection of a straight correlation line with the signal axes. A corresponding example is shown in figure 9. The same method can be employed for multielement samples, too, when an appro-

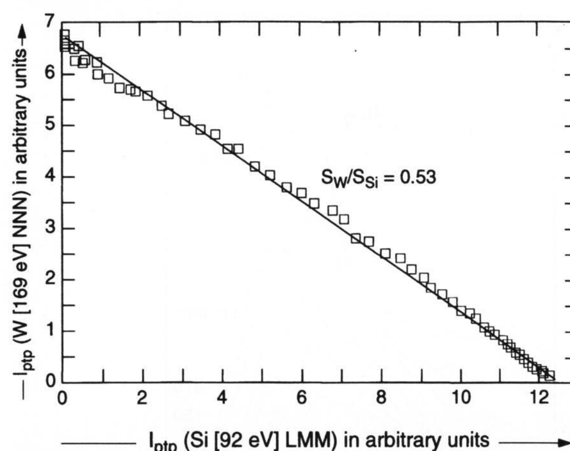

Figure 9. Correlation plot between characteristic AES peaks for wolfram and silicon taken across an interface in a wolfram–silicon multilayer during sputter removal. The relative detection factor between wolfram and silicon for that sample is determined as given in the figure. (Measurement by J. Scholtes, IFOS.)

priate regression technique is applied [20]. Such a direct determination of sensitivity factors is, of course, only possible when chemical influences changing peak positions and intensities can be disregarded.

3.2.3 AES analysis of dielectric samples

While charging effects have been mentioned to be less detrimental in X-ray-induced PES (section 3.1), they can completely deteriorate the Auger spectra because of the low energies of the signal-carrying electrons in this case. AES is, therefore, often considered to be not applicable to electrically nonconducting sample structures. Such difficulties have been shown to be successfully surmounted in the following way [21]:

Quite obviously, no net charging of a dielectric sample occurs when the electron currents to and from the surface compensate each other precisely. Hence, such primary beam parameters have to be selected for which the total secondary electron yield γ, which is known to vary with the energy E_p and the incidence angle of the primary electron beam, becomes unity. As a necessary condition, firstly γ_{max} must be above 1. Secondly, to arrive at stable conditions, the primary beam parameters have to be chosen such that the yield curve $\gamma(E_p)$ crosses unity with a negative slope, i.e. after having passed through its maximum (figure 10). When E_p is chosen slightly above the particular value denoted by E_{II} in figure 10, the dielectric sample will charge up negatively and thus decelerate the primary electrons back to E_p = E_{II} in a self-stabilizing manner. When, on the other hand, the primary electron energy E_p is slightly below E_{II}, the positive charge developing at the surface will retain slow secondary electrons and, hence, bring the effective secondary electron yield back to 1 again. It should be noted that such stable conditions will not establish at E_I where the secondary electron yield curve crosses unity in its rising part.

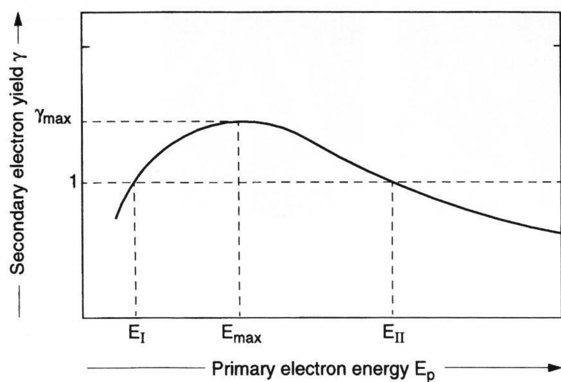

Figure 10. Schematic plot of the variation of the secondary electron yield γ with the primary electron energy E_p.

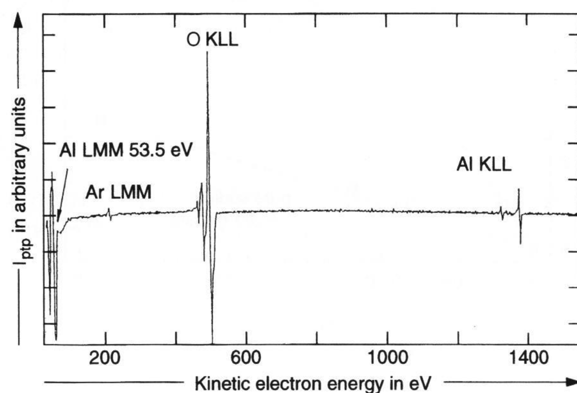

Figure 11. AES survey of an α-Al_2O_3 surface in the differentiated mode. Excitation by a 3 keV primary e^--beam under 50° against the normal to the sample surface. (Measurement by U. Rothhaar, IFOS.)

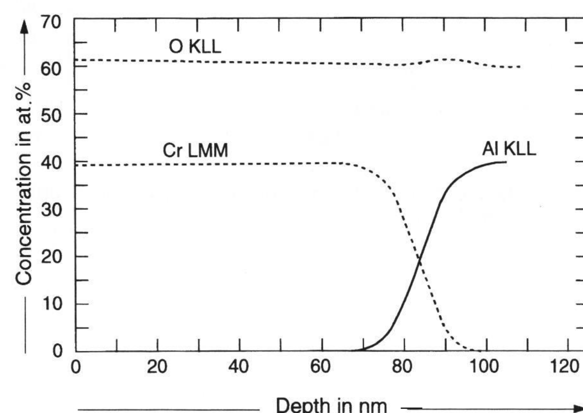

Figure 12. AES concentration sputter depth profile through a Cr_2O_3 layer on α-Al_2O_3. Analysis conditions as for figure 10. (Measurement by U. Rothhaar, IFOS.)

Figure 11 displays the relevant section of an Auger spectrum obtained by this procedure from an α-alumina surface as an example for an almost perfect electrical insulator. The peak positions and the complete appearance of the spectrum are of the same quality as obtained for electrically conducting samples. In the present example, an E_p value of 3 keV and an electron incidence angle of 50° against the surface normal had to be selected.

Under such conditions, Auger sputter depth profiling of coatings on highly insulating materials can be performed in the same way as for conducting samples. This is demonstrated by figure 12 which shows a concentration depth profile of a Cr_2O_3 layer on α-Al_2O_3 as determined from AES sputter depth profiling using the same primary beam parameters as for figure 11. As another example, the charge compensation procedure described here has been applied to the Auger analysis of glass samples (glass SK 16 from Schott Glaswerke, Mainz (Germany)) [21]. Sample charging has to be carefully avoided for such materials, as a field-induced drift of highly mobile ionic constituents like alkali ions causes an immediate deterioration of the surface composition.

4. Mass spectrometric analysis of dielectric surfaces and thin film structures

4.1 Secondary ion mass spectrometry

The application of Secondary Ion Mass Spectrometry SIMS to nonconducting samples becomes difficult for twofold reasons: Firstly, extensive charge is transferred to the sample by the primary ion beam, and secondly, the kinetic energy of the analyzed positive or negative secondary ions is strongly influenced by any sample charging. This may considerably affect the height of the secondary ion signals, e.g. via energy-dependent effects on the transmission of the mass spectrometer. Recent SIMS instruments contain, therefore, an additional low-energy electron gun, from which charge-compensating electrons are conducted to the analyzed surface area. Thus, SIMS can be applied to nonconducting samples, too. Nevertheless, the well-known problems with the quantification of secondary ion signals due to the matrix effect are left, which are known to be particularly stringent for compound materials containing oxidic constituents of different kind and of varying concentration.

SIMS, therefore, delivers in general only a qualitative information about the surface composition. An example is shown in figures 13a and b which were obtained with a recent SIMS-Time-of-Flight Mass Spectrometer (TRIFT by C. A. Evans Ass./Physical Electronics, Eden Prairie (USA)). A 20 keV Ga^+ beam of 1 μm in diameter has been raster-scanned across a bundle of glass fibers which were expected to be coated by copper. A comparison of the secondary ion images for Si^+ (figure a) and Cu^+ (figure b) displays significant differences which demonstrate that a number of the fibers were not or only partially coated.

With regard to its quantification problems a more detailed discussion of the SIMS technique is not included here. In the following the author concentrates on mass spectrometric techniques for surface and thin film analysis utilizing postionized sputtered neutrals, i.e. on SNMS. Also, the recently more closely addressed MCs^+ method (M stands for an elemental constituent of the sample) will be elucidated to some extent, though utiliz-

ing a kind of "secondary" ions which, however, have been shown to form via a chemi-ionization process being deliberately rated as a postionization process, too.

4.2 Surface analysis by MCs^+ ions

When a Cs^+ ion beam is applied to a surface to be analyzed, MCs^+ ions are detected in the particle flux from the sample besides atomic and other molecular ions. Quite recently, the formation of MCs^+ ions has been shown to be controlled by a combination process between a backscattered or re-ejected Cs^+ ion and a simultaneously sputtered neutral atom, M^0, i.e. by

$$M^0 + Cs^+ \rightarrow MCs^+ \; . \tag{7}$$

Evidence for this process results clearly from a strong correlation between the MCs^+ intensities and the atomic polarizability of M^0 for a large number of elements [22]. The Cs^+ ion polarizes a simultaneously ejected neutral surface atom, and the particular MCs^+ ion is formed by an ion-dipole interaction. The still very close surface may act as a third partner which accepts a part of the excess energy from the particular combination process.

Since the flux of sputtered neutral surface atoms is known to be insensitive to the matrix effects in secondary ion emission, the formation mechanism described by equation (7) is expected to be less sensitive to the actual chemical surface conditions. Hence, the MCs^+ signals should provide a much better quantifiability than ordinary SIMS signals. Such a behavior has been confirmed by a number of recent applications of the MCs^+ method also for the analysis of nonconducting samples, when surface charging is compensated with an additionally applied electron beam in the usual way. In comparison with SIMS, the respective sensitivity factors have been found to depend only moderately on the nature of the sample. Residual effects are essentially due to the influence of the actual surface conditions onto the formation of the Cs^+ ions controlling the combination process according to equation (7). Hence, quantitative surface analysis with the MCs^+ method becomes possible with a relatively good reliability.

An example is presented in figures 14a and b. Quite a number of glass samples for which the individual compositions had been specified by the manufacturer were analyzed with regard to their content of alkali metals and of oxygen. The ratios of the respective MCs^+ signals display a good linear correlation with the concentration ratios as received from the producer. Of course, the slope of the straight lines in figures 14a and b supplies with the respective relative detection factors, i.e. for sodium and potassium against oxygen in the present case, which, however, are still found to depend on the nature of the glass sample for reasons already mentioned above. Nevertheless, analytical results as those depicted in figures 14a and b indicate that the MCs^+ method may develop to a useful technique for mass spectrometric surface analysis.

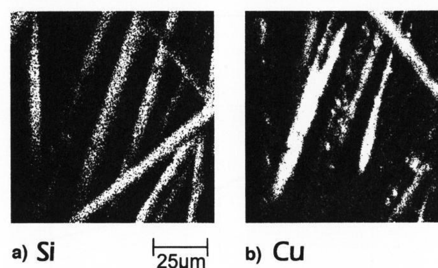

Figures 13a and b. Secondary ion micrographs across a bundle of partially copper-coated glass fibers acquired with a time-of-flight mass spectrometer, a) for Si^+ ions, b) for Cu^+ ions. (Measurement by M. Wahl, IFOS.)

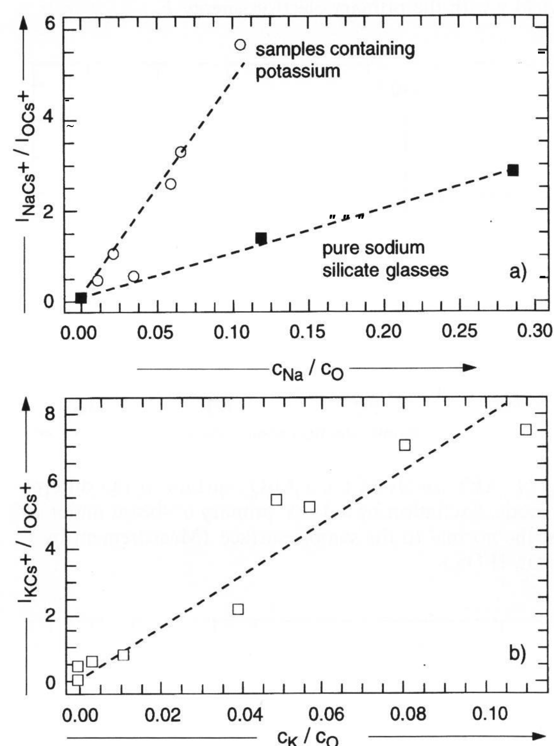

Figures 14a and b. Intensity ratios of MCs^+ signals from different glass samples versus the respective concentration ratios as supplied by the manufacturer, a) results for two different series of glass samples with sodium taken for M, b) results for different samples of the same glass type with potassium taken for M. (Measurement by M. Haag, IFOS.)

4.3 Secondary neutral mass spectrometry

It is well established that even for ionic targets like metal oxides or glass surfaces, secondary ions contribute only by a fraction up to some 10^{-2} to the particle flux released under ion bombardment. Hence, the vast majority of sputter-removed particles consists of neutral atoms and molecules also in such cases. The flux of sputter-ejected secondary neutrals, therefore, reflects the true surface composition, even when the secondary ion signals vary by orders of magnitude with changing chemical conditions at the sample surface. However, in order to allow their mass spectrometric identification, the ejected neutrals must be postionized in an appropri-

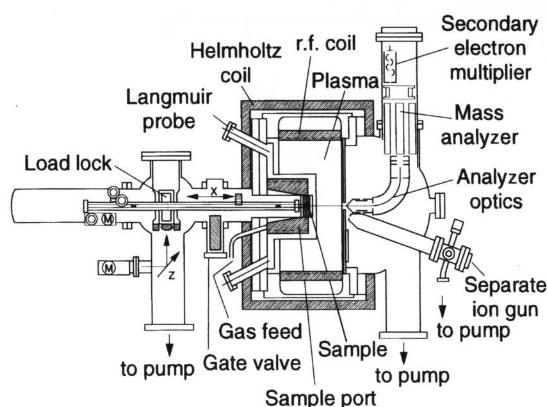

Figure 15. Schematic of an SNMS spectrometer (INA 3 from Leybold/Specs, Leybold AG, Hanau (Germany)).

ate way. While in SIMS particle ejection and ionization occur in the same event, they are strictly separated in SNMS as the essential difference to SIMS. This means that the particle-specific postionization probability in SNMS becomes a constant of the analytical apparatus which makes a quantification of the SNMS signals, i.e. their correlation to the actual surface concentrations, straightforward and simple.

The acronym SNMS was at first introduced to denote a surface analytical technique in which postionization of the sputter-removed neutral surface particles is performed by electron impact ionization in a dense and "hot" electron gas [2, 5 and 14]. In the respective SNMS instruments such an electron gas with electron temperatures T_e corresponding to about 10 eV is provided by the electron component of a low-pressure high-frequency plasma maintained mainly in argon by a specific electrodynamic resonance effect. The postionization probability for a neutral sputtered particle entering the postionization region with energies in the order of a few electronvolts is as high as several 10^{-2}, i.e. by a few orders of magnitude above that with electron beam arrangements used for the same purposes.

More recently, when high-power lasers with sufficiently high photon energies became available, photoionization based on resonant or nonresonant multiphoton absorption schemes is employed as another effective postionization technique. In respective instruments the postionizing laser pulse is simultaneously used as the starting signal for a bunch of postionized particles entering a time-of-flight mass spectrometer. Because of the "parallel" particle detection which becomes thus possible, the consumption of sample material is largely reduced as one of the main advantages of "laser" SNMS [23]. However, in view of the complexity of photoionization processes, the quantification of photoion signals is much less straightforward than in the case of electron impact ionization. Hence, photoionization studies of sputtered neutral atoms or molecules are still a subject of fundamental research, and laser SNMS is not yet employed as a routine technique in practical surface analysis.

In contrast, SNMS spectrometers employing electron gas postionization – nowadays often denoted as e-gas SNMS – are largely used for practical analysis. Their application especially to nonconducting samples will be emphasized here.

4.3.1 Instrumentation and experimental procedure of e-gas SNMS

The technical scheme of an SNMS instrument based on electron gas postionization is displayed in figure 15. The most essential component is the SNMS plasma with an electron density in the order of 10^{11} cm^{-3} at pressures slightly below or above 10^{-3} mbar when operated in argon. The high electron density results from space charge compensation by the background of the positive plasma ions (Ar^{+}), which on the other hand provide an ion reservoir for the bombardment of the sample surface, too. In the direct bombardment mode (DBM), plasma ions are accelerated onto the sample surface by a simple ion optics mounted on top of the sample holder. Sample bombardment becomes then possible with extremely high lateral homogeneity at ion energies down to the 10^2 eV regime at current densities in the order of 1 to 2 mA cm^{-2}.

Alternatively to DBM the sample can be bombarded with a separate ion gun by which a moderately focused ion beam is directed onto the sample surface through the postionizing plasma (separate bombardment mode (SBM), see the ion gun in figure 15 [24]). This technique can be readily employed for the analysis of dielectric surfaces, since the ion charge transported to the sample surface by the external ion beam is instantaneously compensated by a corresponding local variation of the electron retardation current which arrives at the sample surface out from the SNMS plasma. Special care, however, has to be taken in order to avoid a possible superposition of secondary ions to the SNMS signals in this case.

In another ion gun-operated mode of e-gas SNMS, the sample is positioned outside the postionization chamber and bombarded with a conventional ion gun (External Bombardment Mode (EBM) [5 and 24]). Sputter-released neutral surface particles enter the postionizing chamber through an electrical "diaphragm", which can be opened for an electron flow out of the SNMS plasma for compensating surface charging during the analysis of an insulating sample. Both ion beam techniques of SNMS suffer, however, from reduced signal intensities in comparison with DBM or the novel operation mode discussed in section 4.3.2.

4.3.2 Novel high-frequency mode of SNMS

In the past few years the so-called high-frequency mode (HFM) of SNMS has been developed as a novel method for the analysis of dielectric samples [25]. For this operation mode a square-wave high-frequency voltage is applied to the sample instead of a constant d.c. voltage as

in DBM. Such a high-frequency voltage can be basically looked at as a d.c. voltage providing constant ion optical conditions for homogeneous ion bombardment which is switched off periodically to admit short pulses of plasma electrons onto the insulating sample for compensating the positive charge from the preceding ion bombardment interval. The frequency of the applied square-wave high-frequency voltage and the time intervals for the ion and the electron flux within each period have to be chosen such that the variation of the surface potential due to charging up during the ion bombardment interval remains negligibly small. The bombarding ion energy is then controlled by the high-frequency amplitude and, most importantly, the same conditions for the analysis of dielectric samples are achieved with HFM as for conducting samples with conventional DBM.

The application of HFM is elucidated by figures 16a and b and 17. In figures 16a and b step profilometer measurements of the edge sections of bombarding craters obtained with DBM for a conducting sample, and with HFM for an electrically nonconducting glass are compared. Figure 17 displays the SNMS spectrum obtained with the HFM technique for a completely nonconducting ceramic ($BaTiO_3$). Despite the periodically interrupted ion bombardment with Ar^+ ions of only 800 eV the signal intensities for the main components of that sample approach 10^6 cps.

An example for the application of the novel HFM technique to the analysis of a layer structure is presented in figure 18. During the depth profile analysis of a silver–copper double layer on glass for heat protection no electric current was transported through the dielectric substrate. The example in figure 18 demonstrates that sputter depth profiling with HFM becomes possible under conditions comparable to those for conducting sample structures, even when the dielectric properties of the sample vary by orders of magnitude as between the metal layers and the glass substrate in the present case. The HFM version of e-gas SNMS was also successfully used for the depth-dependent analysis of oxide coatings deposited with an alkoxide-gel dip technique on different glass substrates [26].

While the interface width in the example from figure 18 is still in the order of 10 nm and, therefore, not appropriate to demonstrate the depth resolution achieved with HFM, a sophisticated example in that context is presented in figure 19. For the respective measurements a sputter-deposited wolfram–silicon multilayer stack with a double layer thickness of only 3.6 nm on a flat silicon wafer was mounted on an electrically insulating support and depth-profiled with Ar^+ ions of 420 eV. The individual sublayers with a thickness of less than 2 nm corresponding to 6 to 8 atomic layers are almost ideally resolved down to the silicon substrate. This demonstrates that the same high depth resolution as achieved with DBM according to figure 2 becomes possible with HFM for electrically insulating layer structures as well.

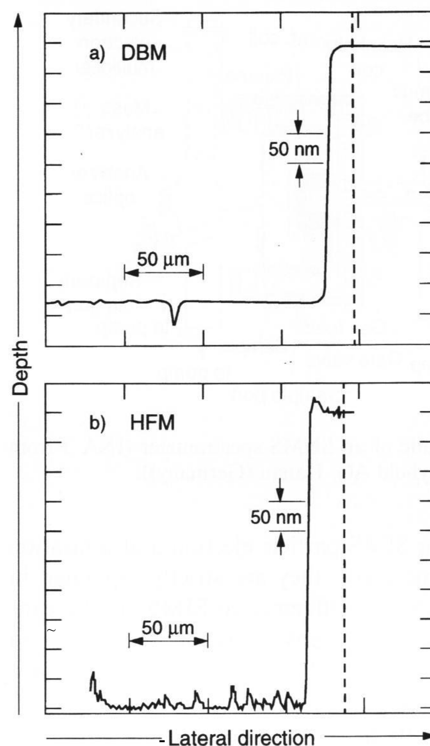

Figures 16a and b. Edge regions of craters produced in amorphous silicon by the conventional DBM technique with 200 eV Ar^+ ions (figure a) and in a nonconducting silicate glass by the novel HFM mode of SNMS with 480 eV Ar^+ ions (figure b).

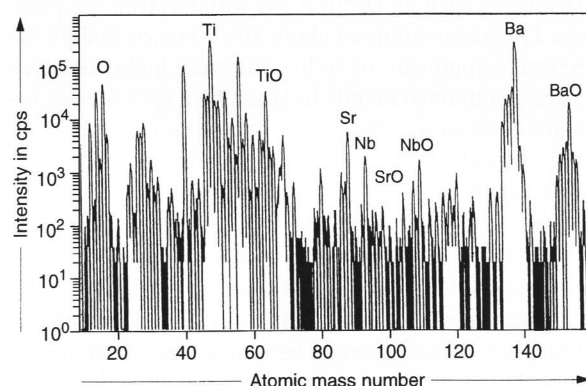

Figure 17. SNMS spectrum of a ceramic $BaTiO_3$ sample containing a number of minor admixtures, acquired with the novel HFM mode of SNMS (normal bombardment with 800 eV Ar^+ ions, operation frequency 500 kHz, ratio of ion-to-electron flux intervals 1 : 1). (Measurement by W. Bock, IFOS.)

4.3.3 Quantification of SNMS

The simple quantifiability of SNMS which is expected from the separation between particle ejection and ionization has been demonstrated by many examples. The basic relation for the SNMS signal $I(X^0)$ of a neutral species being sputter-removed is given by

$$I(X^0) = I_p \, Y_X \, \alpha_X^0 \, \eta_X (1 - \alpha_X^+ - \alpha_X^-) \, . \tag{8}$$

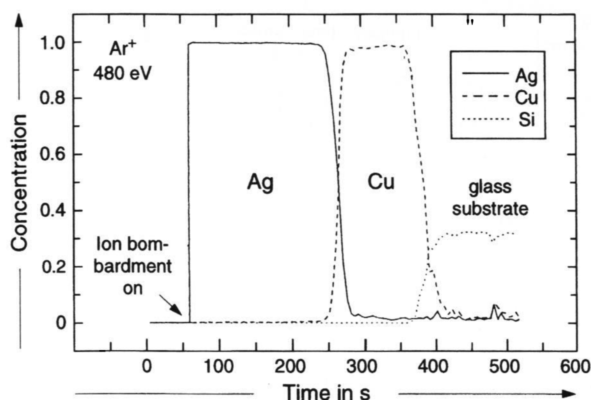

Figure 18. SNMS depth profile analysis of a silver–copper double layer on a dielectric glass substrate with the novel high-frequency mode HFM. Nominal layer thicknesses: 200 nm for silver and 100 nm for copper. (Analysis by M. Kopnarski, IFOS.)

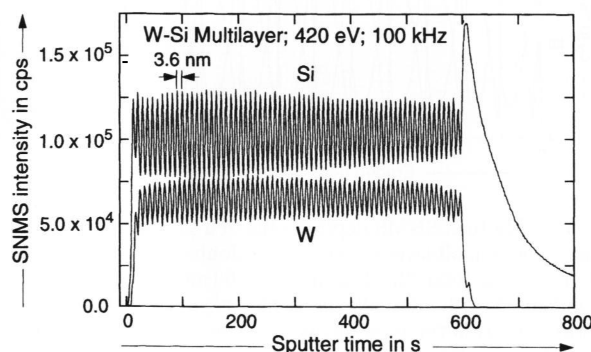

Figure 19. HFM depth profile of a wolfram–silicon multilayer with a double layer thickness of 3.6 nm. The sample was mounted on an electrically insulating ceramic support to which a square-wave high-frequency voltage of 100 kHz with an amplitude of 420 V was applied. (Measurement by W. Bock, IFOS.)

I_p stands for the bombarding ion current and η_X for the detection efficiency of a postionized particle X. The important quantity carrying the analytical information is the partial sputtering yield Y_X which for atomic sputtering under steady state conditions can be expressed as

$$Y_X \equiv c_X Y_{tot} , \tag{9}$$

where Y_{tot} is the total sputtering yield under the respective bombarding conditions.

In equation (8) the SNMS signal $I(X^0)$ is corrected with regard to those particles contributing to Y_X as positive or negative secondary ions. As mentioned above, the secondary ion fractions in the sputtered particle flux and, hence, the respective ionization coefficients $\alpha_X^{+,-}$ entering equation (8) are in the majority of all cases much smaller than unity. Hence, the term in parentheses in equation (8) can be neglected without any appreciable loss in accuracy.

When combining the postionization probability α_X^0 and η_X for a specific sputtered species X to one apparatus constant D_X which is the detection coefficient for X in the particular SNMS system, equation (8) can be simplified to

$$I/(X^0) \equiv I_p c_X D_X Y_{tot} . \tag{10}$$

Extracting c_X from equation (10) and taking into account that $\Sigma c_X = 1$, the relation

$$c_X = \frac{I(X_0)/D_X^{rel}}{\sum_i I(X_i^0)/D_i^{rel}} \tag{11}$$

is easily obtained for the concentrations of an atomic constituent X in the sample.

The quantities D_i^{rel} are again relative detection factors, which refer all individual D_X values to the D value of one identical reference element.

As can be seen from figure 20 the SNMS signals are proportional to the respective element concentrations within an often satisfactory degree of accuracy, i.e. without applying any quantification procedure according to equation (11). The results in figure 20 demonstrate that the relative SNMS sensitivity factors for almost all elements across the periodic table agree within a factor of only 2. This can be understood from the integral character of the postionization coefficient α_0^x which is mainly determined by the overlap between the fixed electron energy distribution in the postionizing SNMS plasma and the individual atomic ionization functions Q_i^X. Since the shapes of Q_i^X as a function of the energy of the ionizing electrons do not change considerably from element to element, α_0^x varies only little, too.

4.3.4 Evaluation of molecule signals and standard free depth scaling with SNMS

Two other useful properties of e-gas SNMS should still be mentioned, too.

a) The basic equation (8) is valid also for neutral sputtered molecules. In this case, the influence of electron impact dissociation can be included in the respective detection factors D_X for a molecular species X. As an example, diatomic oxide molecules are sputter-generated via the so-called direct emission process during the analysis of oxidic systems. From the particular formation model the surface oxygen concentration for a binary oxide is obtained from the relation

$$c_O^s = 0.5 \left[1 \pm \left\{ 1 - \frac{I(MO^0)}{I_{max}(MO^0)} \right\}^{1/2} \right] , \tag{12}$$

where M refers to the oxide-forming metal atoms [25]. $I_{max}(MO^0)$ is the maximum SNMS signal for MO which can be shown to refer to $c_O^s = 0.5$ from the direct emission model. Equation (12) has, in particular, been shown to be valid for oxides with a metal component of as high

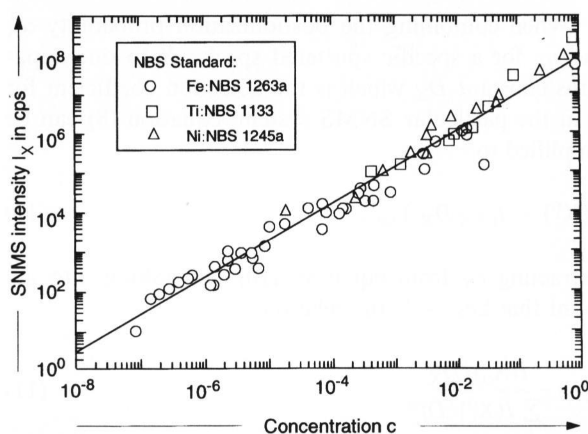

Figure 20. SNMS signals from different standard samples versus the specified concentrations. The results have been obtained with a magnetic sector instrument for e-gas secondary neutral mass spectrometry [28].

Z as Nb_2O_5 or Ta_2O_5. For low concentrations of a reactive species R such as oxygen the direct emission model predicts the surface concentration of R to be proportional to SNMS signal ratio $I(MR^0)/I(M^0)$.

b) Depth profile analysis with SNMS also provides the possibility of determining the absolute depth scale quantitatively from the variation of the SNMS signals themselves [27]. The respective evaluation procedure is based on the characteristic property of SNMS that all sputter-removed particles are collected with individual but constant detection factors.

The time-dependent sputter-eroded depth z is given by

$$z(t) = \int_0^t j_p \frac{Y_{tot}(t')}{n(t')} \mathrm{d}t' \,, \quad (13)$$

where j_p is the bombarding ion current density and n is the time (or depth)-dependent total particle density in the sample. The time-dependent total sputtering yield Y_{tot} can be readily determined by adding together all partial sputtering yields of X derived from the respective SNMS signals at a certain time. The time-dependent sample density can be approached by

$$n(t) = \sum_X c_X(t)\, n_X \,, \quad (14)$$

where $c_X(t)$ is derived from the SNMS signals according to equation (11). For n_X the respective bulk densities of the elemental materials are used as the only approximation entering this depth calibration procedure. By inserting $Y_{tot}(t)$ and $n(t)$ into equation (13) the eroded depth for a certain sputtering time t is exclusively obtained from the time-dependent SNMS signals. An example is given in figures 21a to c again for a tantalum–silicon multilayer system. In that figure the course of the procedure for the determination of the depth scale is elucidated by the sequence of the different panels.

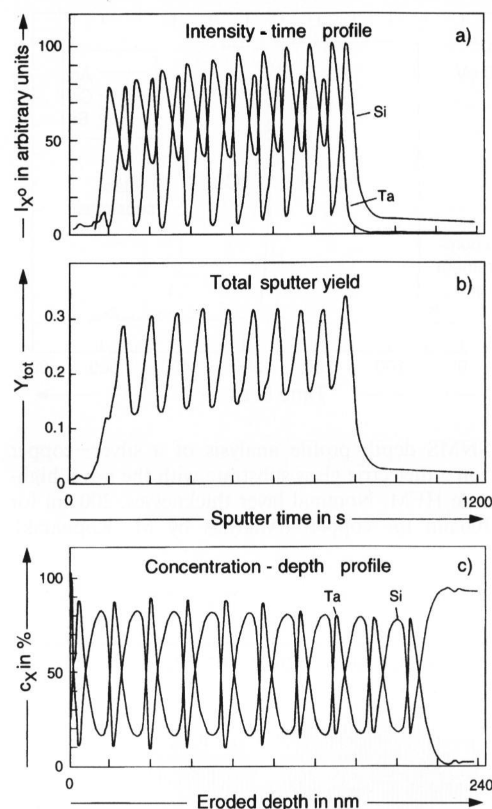

Figures 21a to c. SNMS depth profile of a sandwich-like tantalum–silicon multilayer system with a double layer thickness of 20 nm and a total film thickness of 200 nm. The sample was bombarded with normally incident Ar^+ ions of 250 eV and 1 mA/cm², a) normalized intensities as recorded versus sputter time, b) time-dependent total sputter yield, c) concentration–depth plot evaluated according to equation (13). (Measurement by A. Wucher, Universität Kaiserslautern.)

As a final remark, a new type of e-gas SNMS instrument has to be mentioned [28] which uses a high-transmission magnetic sector spectrometer instead of a quadrupole mass spectrometer as shown in figure 15. With this SNMS instrument, which can be operated in a microprobe mode with a liquid metal ion source as well, SNMS signals up to 10^9 cps are achieved at a background of only $5 \cdot 10^{-2}$ cps. Such numbers result in detection powers around 1 ppb, i.e. only of 10^{13} atoms/cm³ with the full quantifiability of the SNMS technique.

5. List of symbols

A, B	constants in equation (1)
a	monolayer thickness in nm (equation (1))
c_X	(bulk) concentration of species X
c_X^s	surface concentration of species X
D	detection factor in secondary neutral mass spectrometry
d	double layer thickness
d_b	beam diameter (electrons or ions)
E, E_k, E_p, E_0	kinetic energy of electrons or ions in eV
E_b	electron binding energy (related to Fermi level)
F	geometry and efficiency factor
I	signal intensity
j	photon, electron, ion flux or current density

$N(E)$	energy distribution
n_X	particle density of species X in a solid
Q_i^X	electron impact ionization function of species X
S	detection factor in electron spectroscopic methods
T	transmission of analyzer
t	sputtering time
Y_{tot}, Y_X	total and partial sputtering yield
Z	atomic number
z	depth scale
α	bevelling angle in degree
$\alpha_X^{+,-}$	secondary ion formation probability for species X
α_X^0	postionization probability of species X
γ	total secondary electron yield
δl	information depth of a surface analysis method
Δz	absolute depth resolution
η	detection efficiency of a postionized particle X
ϕ	work function
λ	inelastic mean free path in electron emission processes
$h\nu$	photon energy
σ_X	ionization cross-section for atom X

6. References

[1] Briggs, D.; Seah, M. P.: Practical surface analysis. Vol. 1. Auger and X-ray photoelectron spectroscopy. 2nd ed. Chichester, New York: Wiley; Aarau, Frankfurt/M: Salle & Sauerländer, 1990.

[2] Briggs, D.; Seah, M. P.: Practical surface analysis. Vol. 2. Ion and neutral spectroscopy. Chichester, New York: Wiley; Aarau, Frankfurt/M.: Salle & Sauerländer, 1992.

[3] Oechsner, H.: Verfahren zur Untersuchung von Festkörperoberflächen. In: Kohlrausch, F.: Praktische Physik. Bd. 2. 24. Aufl. Stuttgart: Teubner, 1996. p. 717–738.

[4] Feldman, L. C.; Mayer, J. W.: Fundamentals of surface and thin film analysis. Amsterdam (et al.): Elsevier, 1986.

[5] Oechsner, H. (ed.): Thin film and depth profile analysis. Berlin (et al.): Springer, 1984. (Topics in current physics. 37.)

[6] Bartella, J.; Hoffmann, H.; Müller, K. H. et al.: Moderne Verfahren der Oberflächen- und Dünnschichtanalyse. In: Kienel, G. (Hrsg.): Vakuumbeschichtung. Bd. 3. Anlagenautomatisierung, Meß- und Analysentechnik. Düsseldorf: VDI-Verl., 1994. p. 248–335.

[7] Bach, H.; Baucke, F. G. K.: Investigation of glasses using surface profiling by spectrochemical analysis of sputter-induced radiation: I, Surface profiling technique with high in-depth resolution. II, Field-driven formation and electrochemical properties of protonated glasses containing various proton concentrations. J. Am. Ceram. Soc. **65** (1982) no. 11, p. 527–533, 534–539.

[8] Chu, W.-K.; Mayer, J. W.; Nicolet, M.-A.: Backscattering spectrometry. New York (et al.): Acad. Press, 1978.

[9] Teo, B. K.; Joy, D. C. (eds.): EXAFS spectroscopy. Techniques and applications. New York (et al.): Plenum Press, 1981.

[10] Güntherodt, H. J.; Wiesendanger, R. (eds.): Scanning tunneling microscopy. Vol. 1 and 2. Berlin (et al.): Springer, 1992. (Springer series Surface Science. Vol. 20 and 28).

[11] Oechsner, H.: Recent progress in high resolution depth profiling and interface analysis of thin films. Vacuum **37** (1987) p. 763–768.

[12] Seah, M. P.; Dench, W. A.: Quantitative electron spectroscopy of surfaces: standard data base for electron inelastic mean free path in solids. Surf. Interface Anal. **1** (1979) p. 2–11.

[13] Biersack, J. P.; Eckstein, W.: Sputtering studies with the Monte Carlo Program TRIM SP. Appl. Phys. **34** (1984) p. 73–94.

[14] Oechsner, H.: Recent applications of secondary neutral mass spectrometry for quantitative analysis of homogeneous and structured samples. Nucl. Instrum. Meth. Phys. Res. **B33** (1988) p. 918–925.

[15] Stumpe, E.; Oechsner, H.; Schoof, H.: High resolution sputter depth profiling with a low pressure HF-plasma. Appl. Phys. **20** (1979) p. 55–60.

[16] Grunenberg, D.; Sommer, D.; Koch, K. H.: Examinations regarding the correctness of quantitative surface analysis using SNMS. Fresenius J. Anal. Chem. **346** (1993) p. 147–150.

[17] Zalar, A.: Improved depth resolution by sample rotation during Auger electron spectroscopy depth profiling. Thin Solid Films **124** (1985) p. 223–230.

[18] Chastain, J. (ed.): Handbook of X-ray photoelectron spectroscopy. Eden Prairie: Physical Electronics, 1992.

[19] Hedberg, C. L. (ed.): Handbook of Auger electron spectroscopy. 3rd ed. Eden Prairie: Physical Electronics, 1995.

[20] Oechsner, H.: Scanning Auger microscopy. Vide Couches Minces **50** (1994) no. 271, p. 141–150.

[21] Oechsner, H.: Surface and depth profile analyses of insulator materials. In: Proc. 5th Conf. SURTEC, Berlin 1989. München: Hanser, 1989. p. 485–492.

[22] Gnaser, H.; Oechsner, H.: The influence of polarizability on the emission of sputtered molecular ions. Surf. Sci. Lett. **302** (1994) p. L289–L292.

[23] Wucher, A.: Microanalysis of solid surfaces by secondary neutral mass spectrometry. Fresenius J. Anal. Chem. **346** (1993) p. 3–10.

[24] Oechsner, H.: Analysis of insulator samples by secondary neutral mass spectrometry. Scan. Microsc. **3** (1989) p. 411–418.

[25] Oechsner, H.: Secondary neutral mass spectrometry (SNMS) – Recent methodical progress and applications to fundamental studies in particle/surface interaction. Int. J. Mass Spectrom. Ion Processes **143** (1995) p. 271–282.

[26] Ambos, R.; Rädlein, E.; Frischat, G. H.: Surface analysis of sol-gel coatings on glass by secondary neutral mass spectrometry. Fresenius J. Anal. Chem. **353** (1995) p. 614–618.

[27] Wucher, A.; Oechsner, H.: Depth scale calibration during sputter removal of multilayer systems by SNMS. Fresenius J. Anal. Chem. **333** (1989) p. 470–473.

[28] Bieck, W.; Gnaser, H.; Oechsner, H.: Analytical performance of a secondary-neutral microprobe with electron-gas postionization and magnetic-sector mass spectrometer. J. Vac. Sci. Technol. **A12** (1994) p. 2537–2543.

1197P003

Address of the author:

H. Oechsner
Universität Kaiserslautern
Institut für Oberflächen- und Schichtanalytik
Erwin-Schrödinger-Straße
Gebäude 56
D-67663 Kaiserslautern